Minimal bi-6 G^2 completion of bicubic spline surfaces

Kęstutis Karčiauskas[a] and Jörg Peters[b]
[a] Naugarduko 24, Vilnius University, LT-2006, Vilnius, Lithuania
[b] Dept CISE, University of Florida, Gainesville FL 32611-6120, USA, jorg@cise.ufl.edu, tel/fax 352.392.1200/1220

Abstract

This paper addresses a gap in the arsenal of curvature continuous tensor-product spline constructions: an algorithm is provided to fill n-sided holes in C^2 bi-3 spline surfaces using n patches of degree bi-6. Numerous experiments illustrate good highlight line and curvature distribution on the resulting surfaces.

1. Introduction

C^2 tensor-product splines of degree bi-3 are a widely-accepted tool for high-end design. A key challenge is to join with continuity of curvature such patches via n-sided caps where the bi-cubic C^2 tensor-product spline patches do not meet up in a grid-like fashion. The state of the art in constructing *curvature continuous* free-form surface of *least-degree* rely on caps of degree bi-5 consisting of at least $4n$ polynomial pieces [GZ99, Pet02, KP13]. The caps of [GZ99, Pet02] often have poor shape already for moderate valencies. The caps of [KP13] are of high quality but require even more complicated macro-patches when the valence exceeds $n = 7$. The multi-patch constructions of [Pra97, Rei98] of degree bi-6 are the result of composing a bi-3 re-parameterization with a single quadratic polynomial, making such constructions too stiff to model, for example higher-order saddles. If we want to avoid macro-patch splitting of the sectors of the n-sided cap, good results are typically achieved by the construction [LS08] of degree bi-7. For stationary subdivision surfaces, the results of [PR99] imply, again by a composition argument, that bi-6 is a lower bound for C^2 continuity. [KP07, Har11] are examples of C^2 subdivision schemes that use an infinite sequence of contracting polynomial surface rings of degree bi-6 to cover n-sided caps. However, these approaches lack the simplicity of Catmull-Clark-subdivision and are of higher degree than the earlier-mentioned finite-number-of-pieces bi-5 G^2 constructions. 'Almost' G^1 or G^2 constructions, such as [KP15a], that satisfy the smoothness constraints with an error, show promise in practice, but lack a provable bound on the error. The state of the art therefore leaves unresolved the question whether caps for curvature continuous free-form surfaces can be constructed from n polynomial pieces of degree bi-6.

Leveraging the recently-developed and honed kit of techniques for propagating and averaging out data prescribed on the (tensor-border) boundary of a cap, this paper answers the question in the affirmative. The following presents a bi-6 G^2 construction that yields good highlight lines and a good distribution of curvature on a standard gallery of difficult-to-handle input quad meshes [KP15b]. The non-linear constraints underlying the construction can turn out to be infeasible even if there appear to be sufficiently many degrees of freedom and they may result in complicated expressions for any resulting degrees of freedom. Due to the complexity of the calculations both the discovery and the derivation of the algorithm by searching the non-linear space rely heavily on symbolic computation. Moreover, the final derivation of the algorithm with its default values are the result of numerous iterations and experiments that test, on the obstacle course [KP15b], the surface shape resulting from algorithmic variants. Once the default choices and values are in place, it is straightforward to verify curvature continuity by symbolic computation based on the provided coefficients and the concrete algorithm.

Overview. Section 2 lays out the definitions and the setup for the cap construction. Section 3 provides the details and summarizes the algorithm. Section 4 discusses experiments and the rationale underlying choices of default values and it compares the algorithm to alternatives in the literature.

2. Definitions and Setup

We consider the standard setup, an input network of quadrilateral facets or *quads*, ignoring complexities arising from trimming and tolerances. The nodes where four quads meet are called regular. Other are called *irregular nodes*. We assume that each irregular node is surrounded by at least one layer of regular nodes. If the assumption does not hold, one local Catmull-Clark-refinement step achieves this. We denote as *cap-net* $\mathbf{c}$ the two-ring of one irregular node, i.e. the irregular node plus $6n$ nodes forming two layers of quads surrounding it. The second layer of quads may have irregular nodes among its vertices. Fig. 1a displays a cap-net and Fig. 1c displays an *extended cap-net*, i.e. a cap-net plus one additional layer. This additional layer is not used for the construction of the cap but provides a surface ring (green in Fig. 1d) surrounding the cap for a concrete

assessment of the transition. The quality of this transition is as important as the internal quality of the cap. Whenever the context is clear, we abbreviate 'extended cap-net' as *net*.

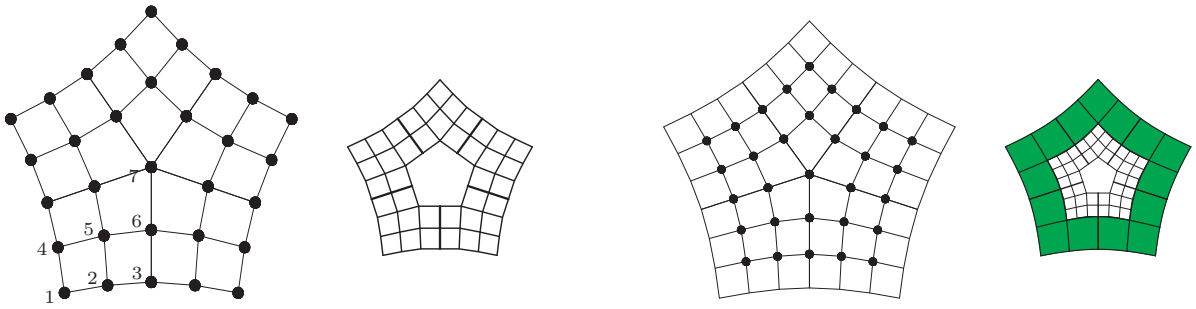

(a) cap-net $\mathbf{c}$ (b) $\mathbf{b}$ (c) extended cap-net (d) bi-3 ring + $\mathbf{b}$

Figure 1: **Input quad mesh.** (a) A cap-net for $n = 5$ or, alternatively, (b) a corresponding tensor-border $\mathbf{b}$ of depth 2 represented as BB-form coefficients of degree 3. (c) An extended cap-net and (d) a regular bi-3 surface ring (green) surrounding the tensor-border.

Each 4×4 sub-grid of points of the network is interpreted as the B-spline control points of a bicubic tensor-product spline surface. The well-known formulas (see e.g. [Far02, PBP02]) for converting the B-spline form to the Bernstein-Bézier form (*BB-form*) can be applied to the cap-net – except at the irregular node. Along the boundary of the cap, this provides second order Hermite data in bi-degree 3 form (fine meshes in Fig. 1b,d). We refer to these Hermite data in the following as the *tensor-border* $\mathbf{b}$ (of depth 2 and degree 3) of the cap construction.

A tensor-product patch $\mathbf{f}$ of bi-degree d is defined by its BB-coefficients $\mathbf{f}_{ij}$ via

$$\mathbf{f}(u,v) := \sum_{i=0}^{d}\sum_{j=0}^{d} \mathbf{f}_{ij} B_i^d(u) B_j^d(v) \;, \quad (u,v) \in \square := [0..1]^2 \;,$$

where $B_k^d(t)$ are the Bernstein-Bézier (BB) polynomials of degree d; e.g. all patches will be parameterized over the unit square.

G^2 continuity of surfaces is achieved by relating adjacent surface pieces via reparameterization ρ so that $\tilde{\mathbf{f}} = \mathbf{f} \circ \rho$. Selecting ρ turns the G^2 constraints into linear constraints and its careful selection is critical for obtaining good properties of the resulting surface cap.

Definition 1. *Two surface pieces $\tilde{\mathbf{f}}$ and $\mathbf{f}$ sharing a curve segment $\mathbf{e}$ along their respective edge join G^2 if there is a suitably-oriented and non-singular reparameterization $\rho : \mathbb{R}^2 \to \mathbb{R}^2$ so that the jets $\partial^k \tilde{\mathbf{f}}$ and $\partial^k(\mathbf{f} \circ \rho)$, $k = 0, 1, 2$, agree along the curve segment $\mathbf{e}$.*

Throughout, we will choose $\mathbf{e}$ to correspond to patch parameters $(u, 0 = v)$. Then the relevant Taylor expansion up to and including degree 2 of the reparameterization ρ with respect to v is

$$\rho := (u + b(u)v + \frac{1}{2}e(u)v^2, a(u)v + \frac{1}{2}d(u)v^2) \;. \tag{1}$$

By the chain rule of differentiation, this yields the well-known G^1 constraints (2) and G^2 constraints (3):

$$\partial_v \tilde{\mathbf{f}} - a(u)\partial_v \mathbf{f} - b(u)\partial_u \mathbf{f} = 0 \;, \tag{2}$$

$$\partial_v^2 \tilde{\mathbf{f}} - a^2(u)\partial_v^2 \mathbf{f} - 2a(u)b(u)\partial_u \mathbf{f}\partial_v \mathbf{f} - b^2(u)\partial_u^2 \mathbf{f} - e(u)\partial_u \mathbf{f} - d(u)\partial_v \mathbf{f} = 0 \;. \tag{3}$$

3. Construction

For the main derivations, we assume that the valence of the irregular node is $n > 4$. Two small changes are needed when $n = 3$. These are listed in Section 3.5. In either case, the cap consists of n patches of degree bi-6. The computations of the first four subsections are illustrated, for $n = 6$, by the Maple script n6 posted next to the manuscript at the second author's web-page. The script allows the reader to provide own input configurations and experiment with functionals other than what we suggest below.

3.1. Reparameterizing between sectors

We consider, for $k \in \{0, \ldots, n-1\}$, two adjacent patches $\grave{\mathbf{p}} := \mathbf{p}^{k-1}$ and $\acute{\mathbf{p}} := \mathbf{p}^{k}$, (superscript modulo n; see Fig. 2a) that share the curve segment $\mathbf{e}(u) := \grave{\mathbf{p}}(u,0) = \acute{\mathbf{p}}(u,0)$ (see Fig. 2b). To avoid bias, we choose the reparameterization (1) along $\mathbf{e}$ to have $a(u) := -1$ and $e(u) := b(u)(b'(u) - \frac{d(u)}{2})$. Testing solvability, enforcing simplicity and comparing the shape of the resulting constructions, yields the carefully calibrated choice

$$b(u) := 2\mathsf{c}(1-u)^2, \quad d(u) := \frac{\delta(1-u)^2}{1-u+\tau u},\ \delta := 24\mathsf{c}(\tau-1), \qquad \text{where } \mathsf{c} := \cos\frac{2\pi}{n}. \tag{4}$$

While $d(u)$ and hence ρ is rational, the surface caps will consist of n *polynomial* patches $\mathbf{p}^k$ of degree bi-6. The choice of $\tau \neq 1$ in the denominator $1-u+\tau u$ is motivated by better shape: numerous examples in Section 4 show that while $\tau := 1$ yields a polynomial ρ, this choice generically results in worse surface shape.

When considering the constraints (2), (3), it is convenient to index the BB-coefficients of the adjacent patches $\grave{\mathbf{p}}$ and $\acute{\mathbf{p}}$ locally, symmetric with respect to sector boundary $\mathbf{e}$ rather than rotationally symmetric about the extraordinary point as is appropriate for the full cap in terms of $\mathbf{p}^k$.

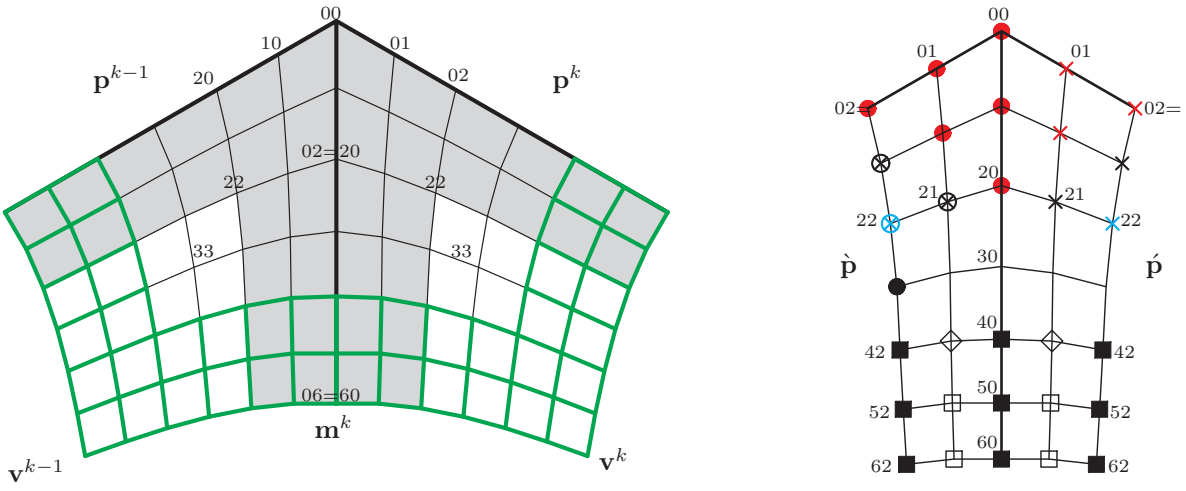

(a) rotationally-symmetric indexing

(b) sector-symmetric indexing

Figure 2: (a) The irregular point has index 00, the curve between two sectors $\mathbf{p}^{k-1}$ and $\mathbf{p}^k$ meets the tensor-border $\mathbf{b}$ at $\mathbf{m}^k$, $\mathbf{v}^k$ denotes the corner point of $\mathbf{p}^k$. (b) The *locally independent* BB-coefficients are marked as disks (black and red), crossed circles (black and cyan) and black squares. All other 16 mesh points represent BB-coefficients fixed in terms of the independent ones to resolve the local G^2 constraints between two sectors.

3.2. Solving the constraints

- By setting
$$\grave{\mathbf{p}}_{30} := \frac{3}{4}(\grave{\mathbf{p}}_{20} + \grave{\mathbf{p}}_{40}) - \frac{3}{10}(\grave{\mathbf{p}}_{10} + \grave{\mathbf{p}}_{50}) + \frac{1}{20}(\grave{\mathbf{p}}_{00} + \grave{\mathbf{p}}_{60}) \tag{5}$$
the degree of $\mathbf{e}$ reduces to 5 and the left-side in (2) becomes a polynomial of degree 6.
- After multiplication by $1-u+\tau u$, the left-side of (3) becomes a polynomial of degree 7. For any other choice of δ the degree would be 8.

To enforce (2) and (3), their $7+8$ BB-coefficients must be set to zero. We solve the corresponding *local* system of 15 linear equations with the symbolic computation system Maple. This allows us to keep many BB-coefficients unassigned for later optimization and only assign the 15 local BB-coefficients that Fig. 2b shows as: hollow squares and diamonds, as uncircled red, black, blue $\times$ or as not marked. (The total count is 16, but recall that $\grave{\mathbf{p}}_{30}$ is defined by (5).) Next, we account for the interactions between these n local systems of equations at the irregular point $\grave{\mathbf{p}}_{00}$, as follows.

(S1) We select the six BB-coefficients $\mathbf{p}^0_{ij}$, $0 \le i+j \le 2$, that define a quadratic expansion of sector $k=0$ at the irregular point and then express the BB-coefficients $\mathbf{p}^k_{ij}$, $0 \le i+j \le 2$, of the other sectors recursively as

$$\begin{aligned}
&\acute{\mathbf{p}}_{00} := \grave{\mathbf{p}}_{00}, \quad \acute{\mathbf{p}}_{10} := \grave{\mathbf{p}}_{10}, \quad \acute{\mathbf{p}}_{20} := \grave{\mathbf{p}}_{20}; \quad \acute{\mathbf{p}}_{01} := -\grave{\mathbf{p}}_{01} + 2\mathsf{c}\grave{\mathbf{p}}_{10} + 2(1-\mathsf{c})\grave{\mathbf{p}}_{00};\\
&\acute{\mathbf{p}}_{11} := -\grave{\mathbf{p}}_{11} + \frac{5\mathsf{c}}{3}\grave{\mathbf{p}}_{20} + 2(1-\mathsf{c})\grave{\mathbf{p}}_{10} + \frac{\mathsf{c}}{3}\grave{\mathbf{p}}_{00};\\
&\acute{\mathbf{p}}_{02} := \grave{\mathbf{p}}_{02} - \frac{24\mathsf{c}}{5}\grave{\mathbf{p}}_{11} + 4\mathsf{c}^2\grave{\mathbf{p}}_{20} + 4(\frac{6\tau\mathsf{c}}{5} - 1)\grave{\mathbf{p}}_{01} + \frac{4\mathsf{c}}{5}(11 - 6(1+\tau)\mathsf{c})\grave{\mathbf{p}}_{10} + 4(1 - \mathsf{c} - \frac{6\tau\mathsf{c}}{5} + \frac{6\tau+1}{5}\mathsf{c}^2)\grave{\mathbf{p}}_{00}.
\end{aligned} \tag{6}$$

The BB-coefficients $\acute{\mathbf{p}}_{01}$, $\acute{\mathbf{p}}_{11}$ and $\acute{\mathbf{p}}_{02}$ of (6) are marked as red crosses in Fig. 2b. Note that this assignment reaffirms the assignment made in the local system but now in dependence on a single sector.

(S2) With $\dot{\mu}_i$, $\ddot{\mu}_i$, $\dddot{\mu}_i$ listed in the Appendix, the constraints for the BB-coefficients marked as black crosses in Fig. 2b are

$$\begin{aligned}\acute{\mathbf{p}}_{21} :=& -\grave{\mathbf{p}}_{21} + (2 - \sum_{i=1}^{5} \dot{\mu}_i)\grave{\mathbf{p}}_{00} + \dot{\mu}_1\grave{\mathbf{p}}_{10} + \dot{\mu}_2\grave{\mathbf{p}}_{20} + \dot{\mu}_3\grave{\mathbf{p}}_{40} + \dot{\mu}_4\grave{\mathbf{p}}_{50} + \dot{\mu}_5\grave{\mathbf{p}}_{60},\\ \acute{\mathbf{p}}_{12} :=& \grave{\mathbf{p}}_{12} + (-\sum_{i=1}^{8} \ddot{\mu}_i)\grave{\mathbf{p}}_{00} + \ddot{\mu}_1\grave{\mathbf{p}}_{01} + \ddot{\mu}_2\grave{\mathbf{p}}_{10} + \ddot{\mu}_3\grave{\mathbf{p}}_{11} + \ddot{\mu}_4\grave{\mathbf{p}}_{20} + \ddot{\mu}_5\grave{\mathbf{p}}_{21} + \ddot{\mu}_6\grave{\mathbf{p}}_{40} + \ddot{\mu}_7\grave{\mathbf{p}}_{50} + \ddot{\mu}_8\grave{\mathbf{p}}_{60}.\end{aligned} \tag{7}$$

This yields a circulant system of $2n$ linear equations for computing $\mathbf{p}_{21}^k$ and $\mathbf{p}_{12}^k$ (since $\mathbf{p}_{21}^{k-1} = \grave{\mathbf{p}}_{12}$, $\mathbf{p}_{12}^{k-1} = \grave{\mathbf{p}}_{21}$, $\mathbf{p}_{21}^k = \acute{\mathbf{p}}_{21}$, $\mathbf{p}_{12}^k = \acute{\mathbf{p}}_{12}$). Similarly, the constraints for the BB-coefficients marked as cyan crosses in Fig. 2b are

$$\begin{aligned}\acute{\mathbf{p}}_{22} :=& \grave{\mathbf{p}}_{22} + (-\sum_{i=1}^{8} \dddot{\mu}_i)\grave{\mathbf{p}}_{00} + \dddot{\mu}_1\grave{\mathbf{p}}_{01} + \dddot{\mu}_2\grave{\mathbf{p}}_{10} + \dddot{\mu}_3\grave{\mathbf{p}}_{11} + \dddot{\mu}_4\grave{\mathbf{p}}_{20} + \dddot{\mu}_5\grave{\mathbf{p}}_{21} + \dddot{\mu}_6\grave{\mathbf{p}}_{40} + \dddot{\mu}_7\grave{\mathbf{p}}_{50} + \dddot{\mu}_8\grave{\mathbf{p}}_{60}\\ &+ \dddot{\mu}_9(\grave{\mathbf{p}}_{42} - \acute{\mathbf{p}}_{42}) + \dddot{\mu}_{10}(\grave{\mathbf{p}}_{52} - \acute{\mathbf{p}}_{52}) + \dddot{\mu}_{11}(\grave{\mathbf{p}}_{62} - \acute{\mathbf{p}}_{62}).\end{aligned} \tag{8}$$

Solving all n constraints of type (8) yields a circulant system of n linear equations for computing $\mathbf{p}_{22}^k$ (since $\mathbf{p}_{22}^{k-1} = \grave{\mathbf{p}}_{22}$, $\mathbf{p}_{22}^k = \acute{\mathbf{p}}_{22}$).

(S3) The assignments, with $\tilde{\mu}_i$, $\bar{\mu}_i$ listed in the Appendix,

$$\begin{aligned}\grave{\mathbf{p}}_{31} :=& (1 - \sum_{i=1}^{6} \tilde{\mu}_i)\grave{\mathbf{p}}_{00} + \tilde{\mu}_1\grave{\mathbf{p}}_{10} + \tilde{\mu}_2\grave{\mathbf{p}}_{20} + \tilde{\mu}_3\grave{\mathbf{p}}_{21} + \tilde{\mu}_4\grave{\mathbf{p}}_{40} + \tilde{\mu}_5\grave{\mathbf{p}}_{50} + \tilde{\mu}_6\grave{\mathbf{p}}_{60}\\ &+ \tilde{\mu}_7(\grave{\mathbf{p}}_{42} - \acute{\mathbf{p}}_{42}) + \tilde{\mu}_8(\grave{\mathbf{p}}_{52} - \acute{\mathbf{p}}_{52}) + \tilde{\mu}_9(\grave{\mathbf{p}}_{62} - \acute{\mathbf{p}}_{62}) + \tilde{\mu}_{10}(\grave{\mathbf{p}}_{22} - \acute{\mathbf{p}}_{22}),\\ \acute{\mathbf{p}}_{31} :=& (1 - \sum_{i=1}^{6} \tilde{\mu}_i)\grave{\mathbf{p}}_{00} + \tilde{\mu}_1\grave{\mathbf{p}}_{10} + \tilde{\mu}_2\grave{\mathbf{p}}_{20} + \tilde{\mu}_3\acute{\mathbf{p}}_{21} + \tilde{\mu}_4\grave{\mathbf{p}}_{40} + \tilde{\mu}_5\grave{\mathbf{p}}_{50} + \tilde{\mu}_6\grave{\mathbf{p}}_{60}\\ &- \tilde{\mu}_7(\grave{\mathbf{p}}_{42} - \acute{\mathbf{p}}_{42}) - \tilde{\mu}_8(\grave{\mathbf{p}}_{52} - \acute{\mathbf{p}}_{52}) - \tilde{\mu}_9(\grave{\mathbf{p}}_{62} - \acute{\mathbf{p}}_{62}) - \tilde{\mu}_{10}(\grave{\mathbf{p}}_{22} - \acute{\mathbf{p}}_{22}),\\ \acute{\mathbf{p}}_{32} :=& \grave{\mathbf{p}}_{32} + (-\sum_{i=1}^{6} \bar{\mu}_i)\grave{\mathbf{p}}_{00} + \bar{\mu}_1\grave{\mathbf{p}}_{10} + \bar{\mu}_2\grave{\mathbf{p}}_{20} + \bar{\mu}_3\grave{\mathbf{p}}_{21} + \bar{\mu}_4\grave{\mathbf{p}}_{40} + \bar{\mu}_5\grave{\mathbf{p}}_{50} + \bar{\mu}_6\grave{\mathbf{p}}_{60}\\ &+ \bar{\mu}_7(\grave{\mathbf{p}}_{42} - \acute{\mathbf{p}}_{42}) + \bar{\mu}_8(\grave{\mathbf{p}}_{52} - \acute{\mathbf{p}}_{52}) + \bar{\mu}_9(\grave{\mathbf{p}}_{62} - \acute{\mathbf{p}}_{62}) + \bar{\mu}_{10}(\grave{\mathbf{p}}_{22} - \acute{\mathbf{p}}_{22})\end{aligned} \tag{9}$$

are purely local to two patches.

(S4) The remaining assignments, depicted as hollow boxes in Fig. 2b are

$$\grave{\mathbf{p}}_{i1} := \grave{\mathbf{p}}_{i0} + \frac{1}{4}(\grave{\mathbf{p}}_{i2} - \acute{\mathbf{p}}_{i2})\,, \quad \acute{\mathbf{p}}_{i1} := \grave{\mathbf{p}}_{i0} - \frac{1}{4}(\grave{\mathbf{p}}_{i2} - \acute{\mathbf{p}}_{i2})\,, \quad i = 5, 6 \tag{10}$$

and, with $w_1 := -\frac{\mathsf{c}}{50\tau}, w_2 := \frac{\mathsf{c}}{50}, w_3 := \frac{\mathsf{c}}{15}$, those for the hollow diamonds are

$$\begin{aligned}\grave{\mathbf{p}}_{41} :=& \grave{\mathbf{p}}_{40} + \frac{1}{4}(\grave{\mathbf{p}}_{42} - \acute{\mathbf{p}}_{42}) + w_1(\grave{\mathbf{p}}_{62} - \acute{\mathbf{p}}_{62}) + w_2(\grave{\mathbf{p}}_{52} - \acute{\mathbf{p}}_{52}) + w_3(\grave{\mathbf{p}}_{60} - \grave{\mathbf{p}}_{50})\,,\\ \acute{\mathbf{p}}_{41} :=& \grave{\mathbf{p}}_{40} - \frac{1}{4}(\grave{\mathbf{p}}_{42} - \acute{\mathbf{p}}_{42}) - w_1(\grave{\mathbf{p}}_{62} - \acute{\mathbf{p}}_{62}) - w_2(\grave{\mathbf{p}}_{52} - \acute{\mathbf{p}}_{52}) + w_3(\grave{\mathbf{p}}_{60} - \grave{\mathbf{p}}_{50}).\end{aligned} \tag{11}$$

3.3. Reparameterizing the tensor-border $\mathbf{b}$

While the assignments (10) match the degree-raised tensor-border $\mathbf{b}$, the assignments (11) are incompatible with a C^2 prolongation of $\mathbf{b}$. Therefore we define, for each edge of a sector, a reparameterization β of degree 4 to adjust $\mathbf{b}$. The BB-coefficients of β are shown in Fig. 3, where an index 00 corresponds to the corner location $\mathbf{v}^{k-1}$ and the index 40 corresponds to the junction $\mathbf{m}^k$ of $\mathbf{e}$ with $\mathbf{b}$ (see Fig. 2a). Setting $a(u) := 1$, $b(u) := 0$ in (1), we get, as required by (10), that β preserves the position and the first cross-derivative along the boundary of $\mathbf{b}$. To satisfy (11) and respect symmetry when switching u and v, we set

$$\begin{aligned}d(u) :=& \sum_{i=0}^{3} d_i B_i^3(u)\,, \quad e(u) := \sum_{i=0}^{4} e_i B_i^4(u), \quad \text{where}\\ d_0 := 0\,,\ d_1 := 0\,,\ d_3 :=& \frac{2\mathsf{c}}{3} + d_2;\ e_0 := 0\,,\ e_1 := 0\,,\ e_2 := \frac{d_2}{2}\,,\ e_3 := \frac{4\mathsf{c}(1-\tau) + \tau d_2}{4\tau}\,,\ e_4 := 0.\end{aligned} \tag{12}$$

The assignments (17) in the Appendix provide the explicit expressions for the coefficients of the so-reparameterized tensor-border.

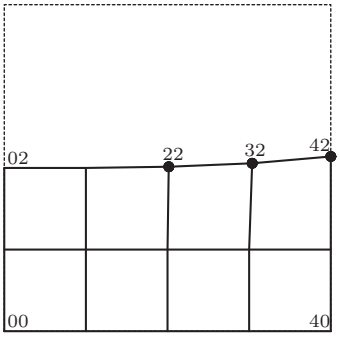

Figure 3: BB-coefficients of the reparameterization β of a sector: the index 00 corresponds to the 'global' location $\mathbf{v}^{k-1}$ in Fig. 2 and index 40 corresponds to $\mathbf{m}^k$; the BB-coefficients not marked by bullets are from the identity map in bi-4 form.

3.4. Solution of the two circulant systems

- The system of $2n$ equations (7) always has a solution. The solution is unique unless $n = 6$. For $n = 6$ we may additionally set one of the BB-coefficients. We choose $\mathbf{p}^0_{21}$.
- The system (8) of n equations can be solved by solving a subsystem of $n-1$ equations in terms of $\mathbf{p}^k_{22}$, $k = 1, \ldots, n-1$, leaving undetermined $\mathbf{p}^0_{22}$. Whatever $\mathbf{p}^0_{22}$, the remaining equation holds if

$$d_2 := \frac{1 - (3 + 2\mathsf{c})\tau + (3 + \mathsf{c})\tau^2}{2\tau^2}. \tag{13}$$

3.5. Construction of 3-sided caps

When $n = 3$, algebraic dependencies require two small changes to the derivation of the constraints and symbolic substitutions. First, the recursive application of formulas (6) requires that $\tau = \frac{4}{3}$. Second, solving the $2n = 6$ equations (7) leaves unconstrained the BB-coefficient $\mathbf{p}^0_{21}$ (as when $n = 6$) so that $\mathbf{p}^0_{21}$, $\mathbf{p}^1_{22}$ and $\mathbf{p}^2_{22}$ are used to solve the $n = 3$ equations (8). In return for having to set $\tau := \frac{4}{3}$, d_2 is unrestricted.

An additional change, to the formula for the irregular point in Step 1 of the Algorithm, is not required but improves the shape.

3.6. The cap construction

Input: A cap-net of $6n + 1$ points $\mathbf{c}^k_j$. $j = 1, \ldots, 7$ with extraordinary node $\mathbf{c}^7 = \mathbf{c}^k_7$, $k = 0, \ldots, n-1$ of valence n (cf. Fig. 1a) – **or** – an n-sided tensor-border $\mathbf{b}$ of degree 3 and depth 2 (cf. Fig. 1b).

Output: A G^2 surface cap, $\mathbf{p}$ consisting of n bi-6 patches joining to $\mathbf{b}$ both C^1 and G^2.

Algorithm

1. For all sectors k, set the irregular point $\mathbf{p}_{00} = \mathbf{p}^k_{00}$ to the limit point of Catmull-Clark subdivision [CC78, HKD93]

$$\mathbf{p}_{00} := (1 - n\nu_5 - n\nu_6)\mathbf{c}^7 + \sum_{i=0}^{n-1}(\nu_5\mathbf{c}^i_5 + \nu_6\mathbf{c}^i_6), \quad \nu_5 := \frac{1}{n(n+5)} + \begin{cases} 1/96 \text{ if } n = 3 \\ 0 \text{ else} \end{cases} \qquad \nu_6 := \frac{4}{n(n+5)}.$$

2. If $n = 3$ then set $d_2^{def} := 0.1$; otherwise use (13). Set a default parameter value $\tau^{def} := \tau_n$ for valence n, where

$$\tau_3 := \frac{4}{3},\ \tau_5 := 0.87,\ \tau_6 := 0.85,\ \tau_7 := 0.84,\ \tau_8 := 0.83,\ \tau_9 := 0.82,\ \tau_{10} := 0.81,\ \tau_{n>10} := 0.8.$$

3. Set the tensor-border of $\mathbf{p}$ to $\mathbf{b} \circ \beta$.

4. Let, for $1 \le i+j \le 2$ and $k = 0, \ldots, n-1$, denote the set of $5+1+n+n = 2n+6$ BB-coefficients

$$\mathcal{P} := \{\mathbf{p}_{ij}^0, \mathbf{p}_{22}^0, \mathbf{p}_{23}^k, \mathbf{p}_{33}^k\}$$

(plus $\mathbf{p}_{21}^0$ if $n = 6$). Express all remaining BB-coefficients in terms of $\mathcal{P}$ and $\mathbf{b} \circ \beta$ to resolve all smoothness constraints. Then $\mathcal{P}$ is determined by minimizing the functional $\mathcal{F}_5$ over all n bi-6 patches,

where

$$\mathcal{F}_\kappa f := \int_0^1 \int_0^1 \sum_{i+j=\kappa, i,j\ge 0} \frac{\kappa!}{i!j!} (\partial_s^i \partial_t^j f(s,t))^2 ds dt. \tag{14}$$

3.7. Implementation via generating functions

The Algorithm works for each coordinate separately. When all cap-net points $\mathbf{c}_m^k$ have value 0, except for $\mathbf{c}_m^0 = 1$ for one of $m = 1, \ldots, 7$ (see Fig. 1a), we obtain the scalar-valued bi-6 coefficients

$$h_{ij}^{k,m} \in \mathbb{R}, \quad k = 0, \ldots, n-1, \ m = 1, \ldots, 7, \ i,j \in \{0, \ldots, 6\}, \tag{15}$$

where $h_{ij}^{0,7} = \ldots = h_{ij}^{n-1,7}$. Then the BB-coefficients of the cap are

$$\mathbf{p}_{ij}^\kappa := h_{ij}^{0,7} \mathbf{c}_7^0 + \sum_{k=0}^{n-1} \sum_{m=1}^{6} h_{ij}^{k,m} \mathbf{c}_m^{\kappa-k}, \tag{16}$$

where the superscript of $\mathbf{c}_m^{\kappa-k}$ is interpreted modulo n.

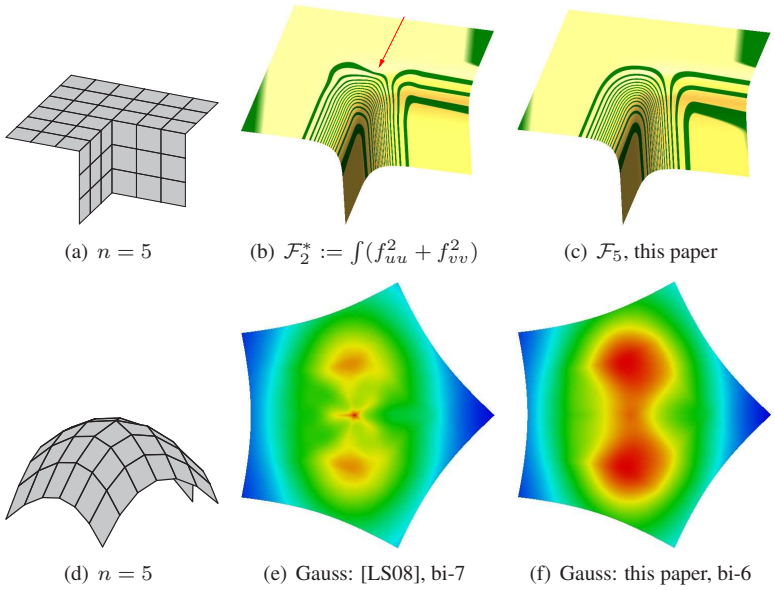

(a) $n = 5$ (b) $\mathcal{F}_2^* := \int (f_{uu}^2 + f_{vv}^2)$ (c) $\mathcal{F}_5$, this paper

(d) $n = 5$ (e) Gauss: [LS08], bi-7 (f) Gauss: this paper, bi-6

Figure 4: **Choice of functional.** Top row: (a) The net of a two-beam-corner. The surface in (b) has its free BB-coefficients set by minimizing $\mathcal{F}_2^* := \int (f_{uu}^2 + f_{vv}^2)$. The arrow points out the flaw in the highlight lines. (c) Our choice $\mathcal{F}_5$ yields more monotone highlight lines. Bottom row: (d) convex net. The Gauss curvature of the bi-7 construction [LS08] shows higher variation than that of our bi-6 construction.

4. Discussion of choices and comparisons

This section discusses the various choices when designing the Algorithm. Since there is no agreement on a mathematical characterization of 'fair shape', these choices are made based on a sequence of challenging input data sets [KP15b]. The goal is to obtain surfaces whose highlight lines do not unnecessarily oscillate or form pinch points.

Fig. 4 illustrates experiments that led to the choice of the functional $\mathcal{F}_5$ when determining the remaining degrees of freedom $\mathcal{P}$ in step 4 of the Algorithm. Clearly, the often-used functional $\mathcal{F}_2^*$ results in undesirable oscillations of the highlight lines (pointed to by the arrow in Fig. 4b), while our choice of $\mathcal{F}_5$, selected as optimal for the input obstacle course [KP15b], does not

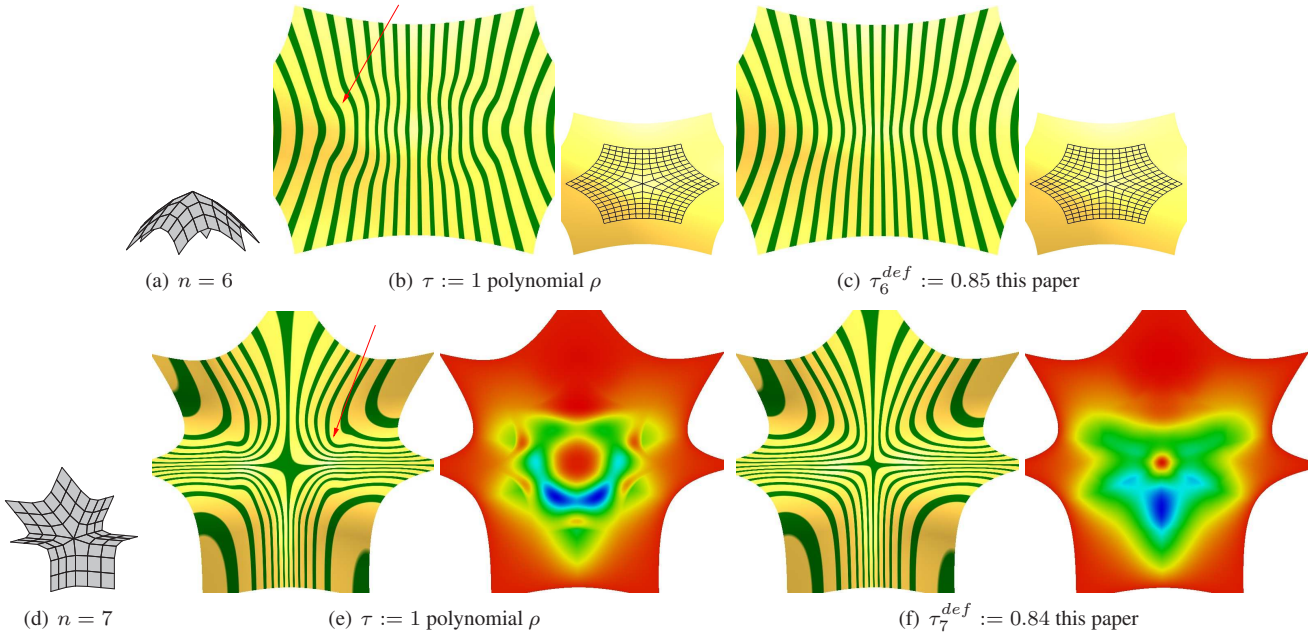

(a) $n = 6$ (b) $\tau := 1$ polynomial ρ (c) $\tau_6^{def} := 0.85$ this paper

(d) $n = 7$ (e) $\tau := 1$ polynomial ρ (f) $\tau_7^{def} := 0.84$ this paper

Figure 5: **Choice of ρ.** (a) Convex net. (b) uses $\tau = 1$, i.e. a polynomial ρ (note the oscillation pointed to by the red arrow) vs. (c) $\tau_6^{def} := 0.85$ yielding the preferred rational ρ of this paper. (d) Saddle net. Subfigures (e) for $\tau := 1$ and (f) for $\tau_7^{def} := 0.84$ display highlight line and Gauss curvature shading. Our choice $\tau_7^{def} := 0.84$ yields a more monotone distribution.

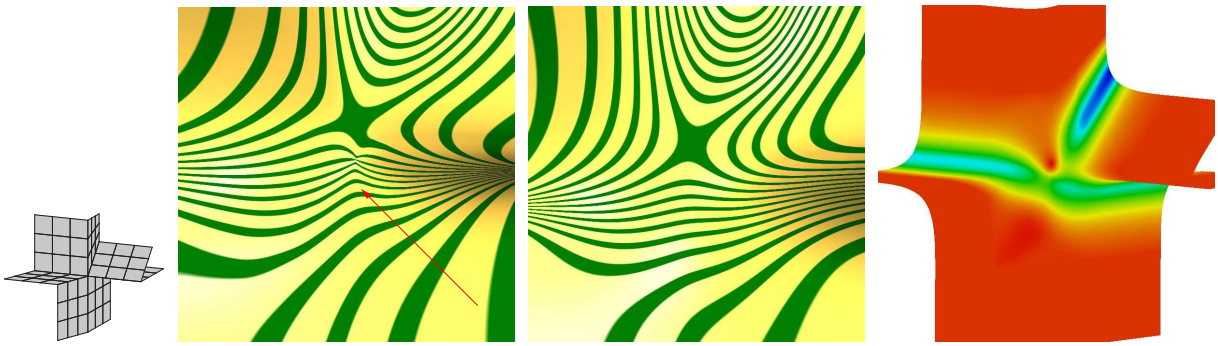

(a) $n = 7$ (b) Catmull-Clark (c) this paper (d) this paper; max curvature

Figure 6: **Comparison to the Catmull-Clark** construction. (a) A sharp 3-beam configuration transformed into an $n = 7$ net; (b,c) zoom into the area corresponding to the bi-6 cap. Note the pinched highlight lines pointed to by the arrow.

(see Fig. 4c). Remarkably, comparing Fig. 4e and Fig. 4f, the curvature of our bi-6 construction is at least as good as that of the bi-7 construction [LS08].

Fig. 5 illustrates the consistent observation of oscillating highlight lines when using a polynomial ρ, i.e. setting $\tau = 1$ (compare Fig. 5b to Fig. 5c). Adjusting the functional does not help: $\tau = 1$ always results in a less uniform distribution of the BB-net of the cap than does τ^{def}. Such a non-uniformity coincides with visible shape artifacts in this and many other test configurations such as Fig. 5e vs Fig. 5f (and Fig. 8o compared to Fig. 8p). We concluded that, while choosing ρ to be polynomial by setting $\tau = 1$ simplifies the constraints, it is not compatible with high-quality surfaces.

Fig. 6 contrasts the new bi-6 surface caps with capping by Catmull-Clark-subdivision. It is well-known that Catmull-Clark-surfaces develop a saddle limit shape even for convex input meshes. However, Catmull-Clark-subdivision also yields pinched highlight lines for inputs such as the net modeling three beams meeting for $n = 7$, Fig. 6a. This confirms that Catmull-Clark-subdivision can not be relied upon to create high-quality surfaces.

Fig. 7 illustrates the importance of choosing the irregular point. In Fig. 7b the irregular point is chosen as part of the optimization. Adjusting the quadratic functional does not help: all fail to prevent the dip. Remarkably, choosing the irregular point to be the Catmull-Clark-limit point (with a small modification when $n = 3$) results in the expected convex shape in the vicinity of the irregular point and class A highlight lines – even though Catmull-Clark-subdivision surfaces itself does not yield

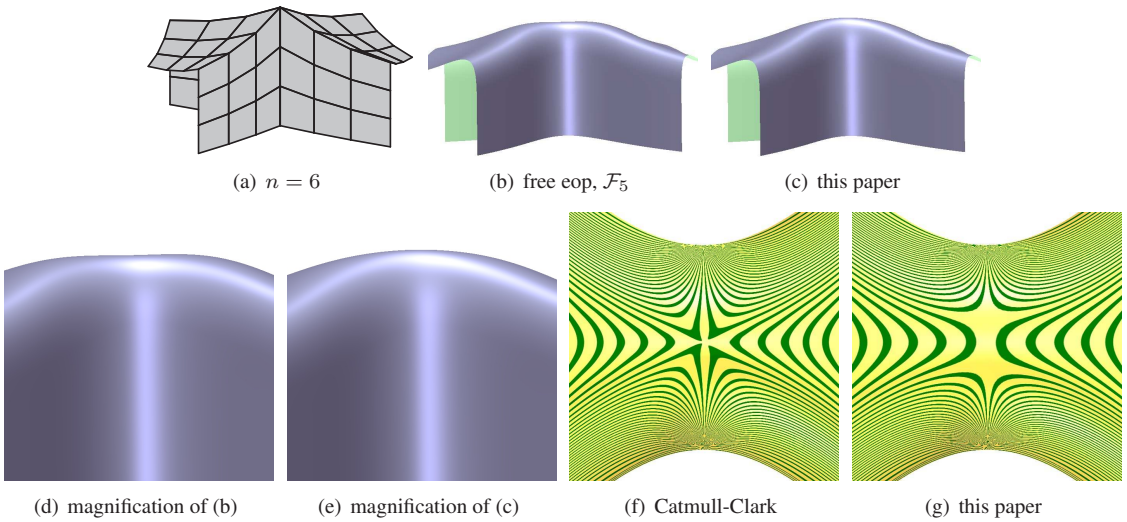

(a) $n = 6$ (b) free eop, $\mathcal{F}_5$ (c) this paper

(d) magnification of (b) (e) magnification of (c) (f) Catmull-Clark (g) this paper

Figure 7: **Choice of irregular point** (eop). (a) an input net indicating a convex irregular point-neighborhood. Setting the irregular point by functionals, here $\mathcal{F}_5$, results in a noticeable dip (b,d) while using the Catmull-Clark-limit point yields the expected shape (c,e). However, using the Catmull-Clark-surface directly does not yield a high-quality surface (f vs g).

class A surface (as is verified also for this example by comparing Fig. 7f to Fig. 7g).

In Fig. 8 the input net is generated by creating a design sketch, i.e. several basic surfaces are placed together without concern for their transition. The sketch is approximated by a B-spline mesh. Any later change of the design corresponding to altering or repositioning the basic surfaces then corresponds to moving groups of control points, as might be done in B-spline based design environments. The sketch Fig. 8a is the result of replacing one quarter of a quadric with a bicubic patch connected via vertical side-walls. Fig. 8b and c show the derived net and the BB-nets of bi-3 ring and the bi-6 cap. The design modifications of Fig. 8e and Fig. 8i illustrate the flexibility and convenience of this approach. Fig. 8k,l show a good distribution of highlight lines even for extreme configurations and high valence $n = 8$. The second design Fig. 8m is sketched by juxtaposing three bi-quadratic and two planar pieces. Its modification trades one bi-quadratic piece for a planar piece.

Valence $n > 8$ is rare in practice. We include examples of valence $n = 9, 10, 12$ in Fig. 9 to confirm that the bi-6 construction can handle also exotic configurations.

When $n = 3$, the juxtapositions of Fig. 10b,c and of Fig. 10e,f demonstrate that the new bi-6 construction has a more uniform curvature distribution than [LS08]. We credit our subtle setting of the irregular point, first used in [KP13] with the improved curvature. For $n = 3$, the G^2 construction in [KP13] uses $d(u) := -4(1-u)^2$ which, just as its more general choice $d(u) := -\frac{4}{1-u+\tau u}(1-u)^2$ yield two fewer unconstrained BB-coefficients than our bi-6 construction. Since all three constructions yield surfaces of similar quality, we believe that the setting of the irregular point is what crucially influences highlight line distribution.

In Fig. 11(a,d,g,k) one node of the characteristic net of Catmull-Clark subdivision is elevated. While artificial, such perturbed planar cap-nets acerbate and reveal, with remarkable clarity, the shortcomings of new and old constructions. For valencies $n = 5, 6$, the constructions of [LS08] and bi-6 still do well, but for $n = 7$ the shape of the new bi-6 construction and for $n = 8$ both [LS08] and the bi-6 construction no longer satisfy the requirement of simple, monotone highlight lines. To understand this better, we consider the circulant systems (7) and (8). As [HPS12] showed, systems of type (7) allow no or little freedom. The non-local interaction of constraints of type (8), however, is specific to constructions of degree bi-6 and lower. The resulting tight interleaving of constraints can lead to unwanted oscillations when $n \geq 7$. Degree bi-7 constructions, such as [LS08], have more local freedom that can improve shape. An even better result is achieved with the G^2 construction [KP13] that uses n macro-patches of 4 (or 7 for higher valences) pieces of degree bi-5. Here, too, the additional degrees of freedom are used to improve the shape.

5. Conclusion

Matching the bi-6 degree lower bound for C^2 subdivision surfaces, the construction of this paper establishes that G^2 free-form surfaces with good curvature distribution can use only *one bi-6 patch per sector*. Among curvature continuous surfaces filling holes in a bi-3 spline complex and using one patch per quad where n quads meet, the new bi-6 construction is likely of minimal polynomial degree to achieve high-quality, i.e. non-oscillating highlight lines. The key ingredients of the construction are its rational reparameterization in the form of a linear denominator in $d(u)$ and the derivation and symbolic solution of the

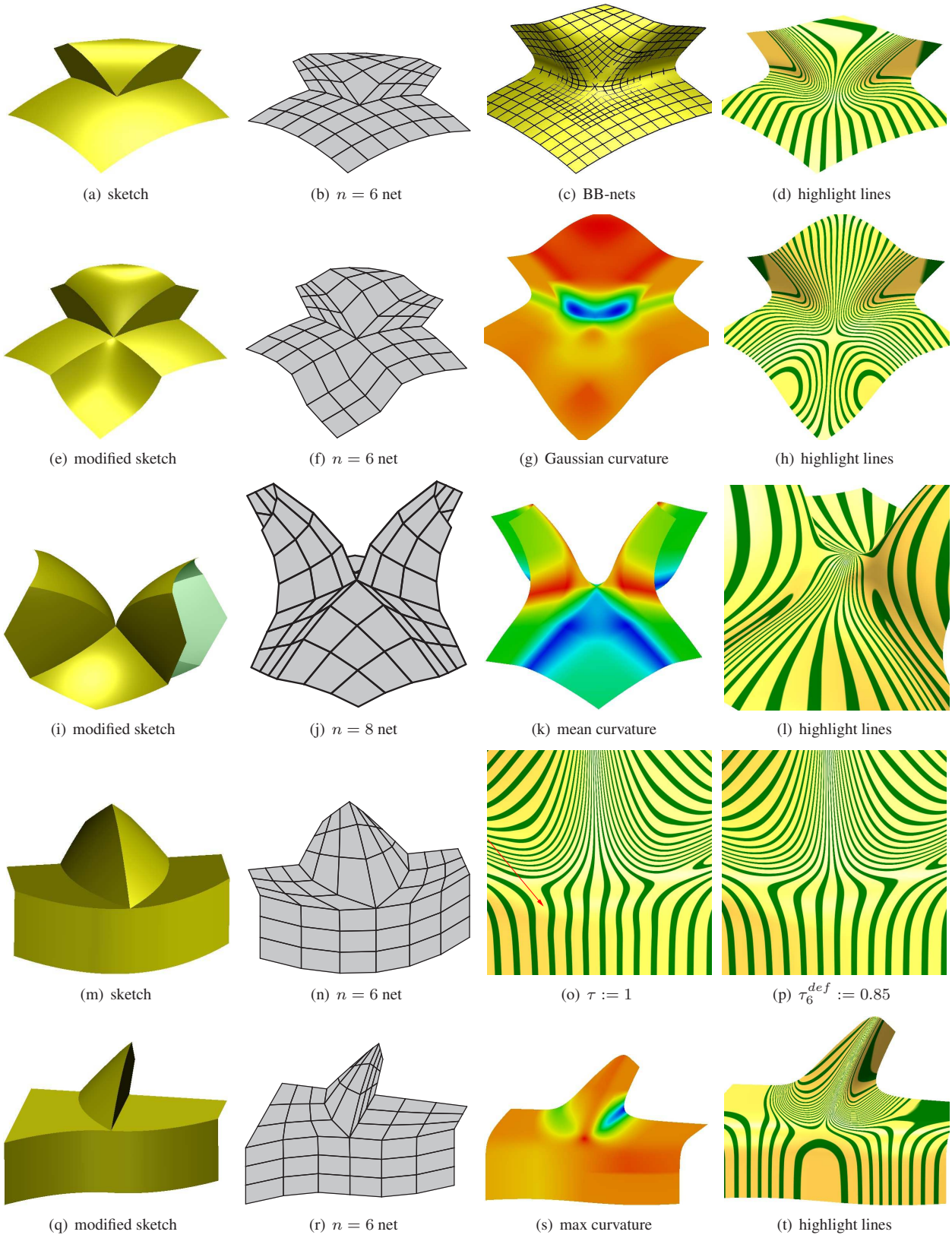

(a) sketch (b) $n = 6$ net (c) BB-nets (d) highlight lines

(e) modified sketch (f) $n = 6$ net (g) Gaussian curvature (h) highlight lines

(i) modified sketch (j) $n = 8$ net (k) mean curvature (l) highlight lines

(m) sketch (n) $n = 6$ net (o) $\tau := 1$ (p) $\tau_6^{def} := 0.85$

(q) modified sketch (r) $n = 6$ net (s) max curvature (t) highlight lines

Figure 8: **Design with simple surfaces** yields challenging input nets.

interlocking sets of G^2 constraints that are circulant systems arising from interaction of local solutions. Discovering formula (13) was crucial to enable a construction of low degree that avoids oscillating highlight lines. Once (13) had been derived, a

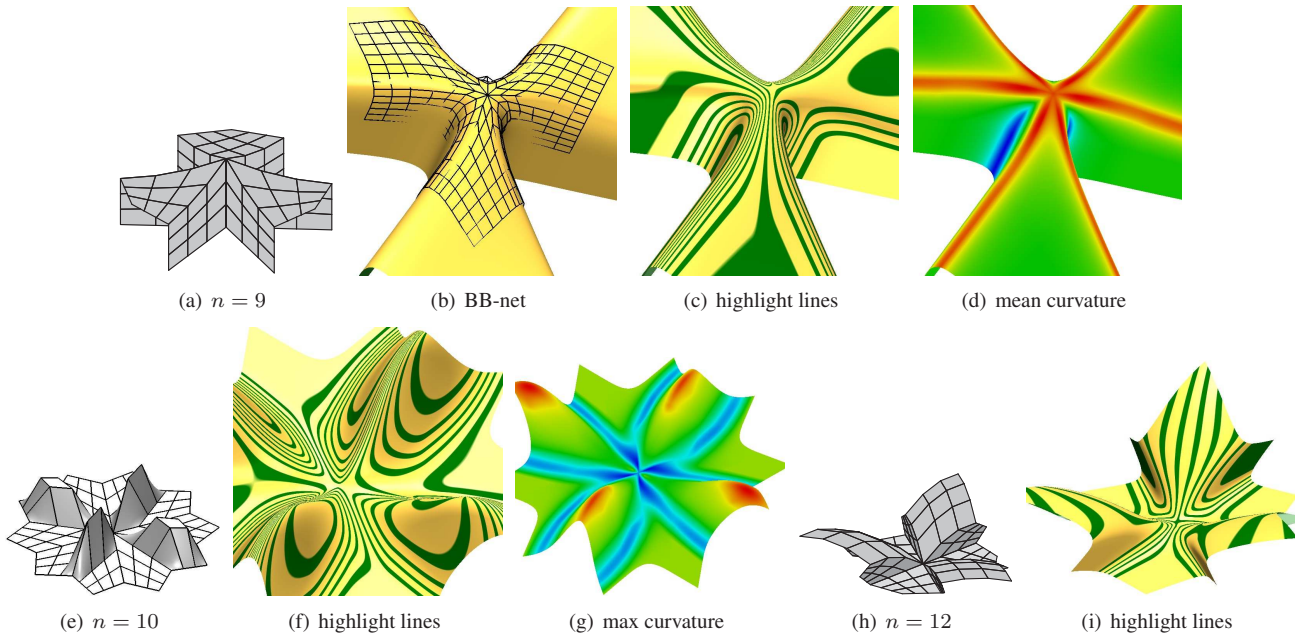

(a) $n = 9$ (b) BB-net (c) highlight lines (d) mean curvature

(e) $n = 10$ (f) highlight lines (g) max curvature (h) $n = 12$ (i) highlight lines

Figure 9: **High valencies** and exotic configurations.

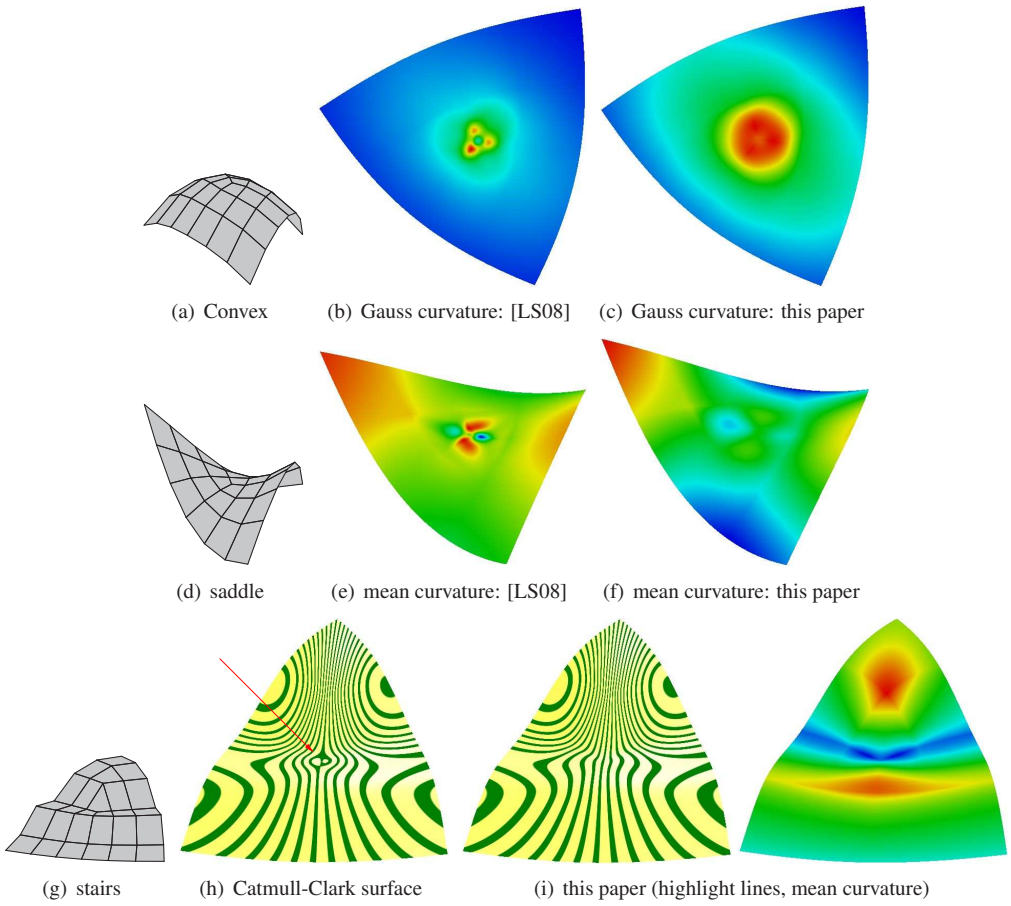

(a) Convex (b) Gauss curvature: [LS08] (c) Gauss curvature: this paper

(d) saddle (e) mean curvature: [LS08] (f) mean curvature: this paper

(g) stairs (h) Catmull-Clark surface (i) this paper (highlight lines, mean curvature)

Figure 10: Valence $\mathbf{n = 3}$. (a) Convex net, the main scenario for valence 3. (d) Saddle net. (g) Stair net.

formal proof of G^2 continuity became possible: we verified symbolically up to valence $n = 16$ and numerically, at 30 digit precision, for $n = 20, 30, 40, 50$.

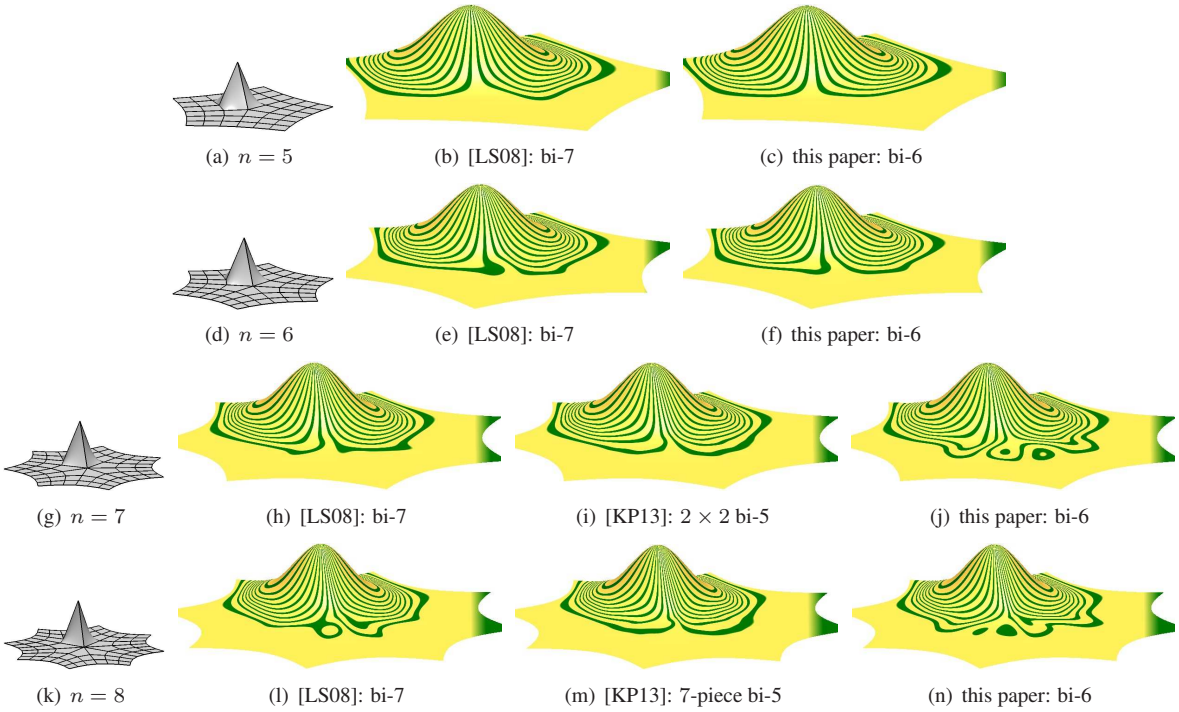

Figure 11: **Limitations** of the bi-6 construction for extreme configurations. Our bi-6 and the bi-7 construction [LS08] fail the oscillation test for high valencies.

Two related questions are still unresolved. First, the tensor-border is often itself the result of approximating rational shapes by piecewise polynomial surfaces. Tensor-borders can therefore in practice be of degree higher than bi-3. Unless one adds one or more bi-3 transition layers, this increased degree of the tensor-border adds new algebraic complexity to the cap construction. A second direction of inquiry is to relax the formal continuity requirements and obtain controllable degrees of freedom for shape optimization. While proving *a priori* bounds on curvature discontinuities in this scenario is a difficult challenge, in practice, such approaches may be effective for the more limited variation of high-quality primary surfaces to be capped (see e.g. [KP15a]).

Acknowledgements.. The work was supported in part by NSF Grant CCF-1117695. Charles Loop kindly provided the generating functions for the comparisons with [LS08].

[CC78] E. Catmull and J. Clark. Recursively generated B-spline surfaces on arbitrary topological meshes. *Computer-Aided Design*, 10:350–355, September 1978.

[Far02] G. Farin. *Curves and Surfaces for Computer Aided Geometric Design: A Practical Guide*. Academic Press, San Diego, 2002.

[GZ99] John A. Gregory and Jianwei Zhou. Irregular C^2 surface construction using bi-polynomial rectangular patches. *Comp Aided Geom Design*, 16(5):423–435, 1999.

[Har11] René Hartmann. *Subdivision Surfaces: C2 schemes and generalized control nets*. PhD thesis, TU Darmstadt/Mathematik, Darmstadt, 2011.

[HKD93] Mark Halstead, Michael Kass, and Tony DeRose. Efficient, fair interpolation using Catmull-Clark surfaces. In *Proc 20th Annual Conference on Computer Graphics and Interactive Techniques*, SIGGRAPH '93, pages 35–44, New York, NY, USA, 1993. ACM.

[HPS12] Tamas Hermann, Jorg Peters, and Tim Strotman. Curve networks compatible with G^2 surfacing. *Computer Aided Geometric Design*, 29:219–230, April 2012.

[KP07] K. Karčiauskas and J. Peters. Concentric tesselation maps and curvature continuous guided surfaces. *Computer Aided Geometric Design*, 24(2):99–111, Feb 2007.

[KP13] K. Karčiauskas and J. Peters. Biquintic G^2 surfaces. In G. Mullineux Robert J. Cripps and M. A. Sabin, editors, *The Mathematics of Surfaces XIV*, pages 213–236. The Institute of Mathematics and its Applications, September 2013.

[KP15a] Kęstutis Karčiauskas and Jörg Peters. Can bi-cubic surfaces be class a? In *SGP 2015, Symposium Geometry Processing 2015, Graz*, July 6-8 2015.

[KP15b] Kęstutis Karčiauskas and Jörg Peters. Quad-net obstacle course, 2015. http://www.cise.ufl.edu/research/SurfLab/shape_gallery.shtml.

[LS08] Charles T. Loop and Scott Schaefer. G^2 tensor product splines over extraordinary vertices. *Comput. Graph. Forum*, 27(5):1373–1382, 2008.

[PBP02] Hartmut Prautzsch, Wolfgang Boehm, and Marco Paluszny. *Bézier and B-spline techniques*. Springer Verlag, 2002.

[Pet02] J. Peters. C^2 free-form surfaces of degree (3,5). *Comp Aided Geom Design*, 19(2):113–126, 2002.

[PR99] Hartmut Prautzsch and Ulrich Reif. Degree estimates for C^k-piecewise polynomial subdivision surfaces. *Adv. Comput. Math*, 10(2):209–217, 1999.

[Pra97] H. Prautzsch. Freeform splines. *Comput. Aided Geom. Design*, 14(3):201–206, 1997.

[Rei98] U. Reif. TURBS—topologically unrestricted rational B-splines. *Constr. Approx.*, 14(1):57–77, 1998.

Appendix

First, we give the explicit formulas for the coefficients in equations (7), (8) and (9). The subscript $1:m$ indicates that elements $1, 2, \ldots, m$ are listed.

$$\dot{\mu}_{1:5} := \frac{2\mathsf{c}}{5},\ 2-\mathsf{c},\ \mathsf{c},\ -\frac{2\mathsf{c}}{5},\ \frac{\mathsf{c}}{15};$$

$$\ddot{\mu}_{1:8} := -\frac{4\mathsf{c}}{5}\tau^2,\ 4(1-\mathsf{c}+\frac{\mathsf{c}^2}{5})+\frac{24\mathsf{c}(\mathsf{c}-1)}{5}\tau+\frac{4\mathsf{c}^2}{5}\tau^2,\ \frac{24\mathsf{c}}{5}\tau-4,\ \frac{2\mathsf{c}}{3}(11-3\mathsf{c}-6\mathsf{c}\tau),\ -4\mathsf{c},\ 2\mathsf{c}^2,\ -\frac{4\mathsf{c}^2}{5},\ \frac{2\mathsf{c}^2}{15};$$

$$\dddot{\mu}_{1:11} := \frac{4\mathsf{c}}{25}\tau^3,\ \frac{4\mathsf{c}}{25}(5-3\mathsf{c}\tau+6(1-\mathsf{c})\tau^2-\mathsf{c}\tau^3),\ -\frac{24\mathsf{c}}{25}\tau^2,\ 4-2\mathsf{c}+\frac{6\mathsf{c}(\mathsf{c}-2)}{5}\tau+\frac{4\mathsf{c}^2}{5}\tau^2,\ \frac{12\mathsf{c}}{5}\tau-4,$$
$$\frac{2\mathsf{c}}{5}(5-3\mathsf{c}\tau),\ \frac{4\mathsf{c}}{25}(3\mathsf{c}\tau-5),\ \frac{2\mathsf{c}}{75}(5-3\mathsf{c}\tau),\ -\frac{3\mathsf{c}}{5\tau},\ \frac{6\mathsf{c}(5-\mathsf{c}\tau)}{125\tau^2},\ \frac{\mathsf{c}(6\mathsf{c}\tau-5)}{125\tau^3};$$

$$\tilde{\mu}_{1:10} := -\frac{11}{20},\ \frac{11\mathsf{c}-10}{8\mathsf{c}},\ \frac{5}{4\mathsf{c}},\ \frac{1}{8}-\frac{\mathsf{c}}{4},\ \frac{3\mathsf{c}}{10}-\frac{1}{20},\ \frac{1}{120}-\frac{\mathsf{c}}{20},\ \frac{3}{8\tau},\ \frac{3\mathsf{c}\tau-15}{100\tau^2},\ \frac{5-6\mathsf{c}\tau}{200\tau^3},\ -\frac{5}{16\mathsf{c}}.$$

$$\bar{\mu}_{1:10} := 1,\ \frac{5(2-\mathsf{c})}{2\mathsf{c}},\ -\frac{5}{\mathsf{c}},\ \frac{5}{2},\ -1,\ \frac{1}{6},\ \frac{3}{10\tau}(\mathsf{c}\tau-5),\ \frac{3}{125\tau^2}(25-20\mathsf{c}\tau+\mathsf{c}^2\tau^2),-\frac{1}{250\tau^3}(25-45\mathsf{c}\tau+6\mathsf{c}^2\tau^2),\ \frac{5}{4\mathsf{c}}.$$

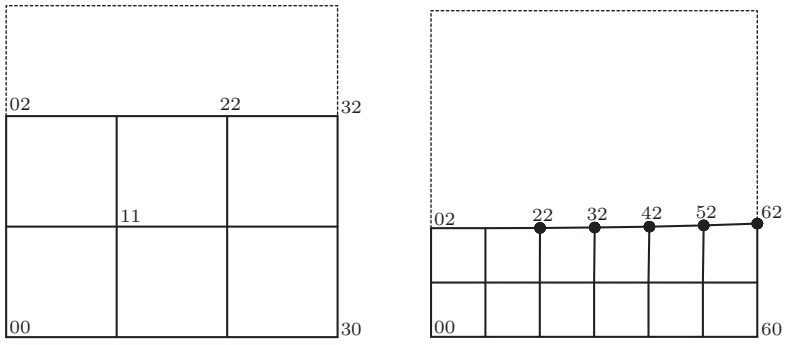

(a) $\mathbf{b}_{ij}$ (b) $\mathbf{q}_{ij}$

Figure 12: **Tensor-border reparameterization.** BB-coefficients $\mathbf{b}_{ij}$ of input tensor-border $\mathbf{b}$ and BB-coefficients $\mathbf{q}_{ij}$ of $\mathbf{b} \circ \beta$.

Next, for the convenience of a reader endeavoring to re-derive the algorithm or check curvature continuity, we present the BB-coefficients $\mathbf{q}_{ij}$, $i = 0, \ldots, 6$, $j = 0, \ldots, 2$ of the reparameterized tensor-border $\mathbf{q} := \mathbf{b} \circ \beta$ where $\mathbf{b}_{ij}$, $i = 0, \ldots, 3$,

$j = 0, \ldots, 2$, are the BB-coefficients of $\mathbf{b}$. Since the position and derivative of $\mathbf{q}$ are just the tensor-border with the degree raised to bi-6, we need only specify the BB-coefficients $\mathbf{q}_{k2}$, $k = 2, \ldots, 6$ (bullets in Fig. 12):

$$\begin{aligned}
\mathbf{q}_{22} &:= \sum_{i=0}^{2}\sum_{j=0}^{2}\gamma_{ij}^{2}\mathbf{b}_{ij},\ \gamma_{ij}^{2} = \gamma_{ji}^{2}; \quad \mathbf{q}_{32} := \sum_{i=0}^{3}\sum_{j=0}^{2}\gamma_{ij}^{3}\mathbf{b}_{ij}; \\
\mathbf{q}_{42} &:= \sum_{i=1}^{3}\sum_{j=0}^{2}\gamma_{ij}^{4}\mathbf{b}_{ij}; \quad \mathbf{q}_{52} := \sum_{i=2}^{3}\sum_{j=0}^{2}\gamma_{ij}^{5}\mathbf{b}_{ij}; \quad \mathbf{q}_{62} := \sum_{j=0}^{2}\gamma_{3j}^{6}\mathbf{b}_{3j},
\end{aligned} \tag{17}$$

where

$$\begin{aligned}
\gamma_{00}^{2} &:= \frac{1-d_2}{25},\ \gamma_{10}^{2} := \frac{6+d_2}{50},\ \gamma_{20}^{2} := \frac{1}{25},\ \gamma_{11}^{2} := \frac{9}{25},\ \gamma_{21}^{2} := \frac{3}{25},\ \gamma_{22}^{2} := \frac{1}{25}; \\
\gamma_{0:3,0}^{3} &:= \frac{(3+5\mathsf{c}-3d_2)\tau - 6\mathsf{c}}{300\tau},\ \frac{(9-2\mathsf{c}-7d_2)\tau + 2\mathsf{c}}{100\tau},\ \frac{9+3d_2}{100},\ \frac{1}{100}; \\
\gamma_{0:3,1}^{3} &:= \frac{18+2\mathsf{c}+3d_2}{600},\ \frac{54+9d_2}{200},\ \frac{27}{100},\ \frac{3}{100}; \quad \gamma_{0:3,2}^{3} := \frac{1}{100},\ \frac{9}{100},\ \frac{9}{100},\ \frac{1}{100}; \\
\gamma_{1:3,0}^{4} &:= \frac{(6+6\mathsf{c}-5d_2)\tau - 8\mathsf{c}}{150\tau},\ \frac{(9-4\mathsf{c}-5d_2)\tau + 4\mathsf{c}}{75\tau},\ \frac{2+d_2}{50}; \\
\gamma_{1:3,1}^{4} &:= \frac{18+2\mathsf{c}+3d_2}{150},\ \frac{18+3d_2}{50},\ \frac{3}{25}; \quad \gamma_{1:3,2}^{4} := \frac{1}{25},\ \frac{3}{25},\ \frac{1}{25}; \\
\gamma_{20}^{5} &:= \frac{(3+\mathsf{c}-2d_2)\tau - 2\mathsf{c}}{30\tau},\ \gamma_{30}^{5} := \frac{(3-2\mathsf{c}-d_2)\tau + 2\mathsf{c}}{30\tau}; \\
\gamma_{21}^{5} &:= \frac{18+2\mathsf{c}+3d_2}{60},\ \gamma_{31}^{5} := \frac{6+d_2}{20}; \quad \gamma_{22}^{5} := \frac{1}{10},\ \gamma_{32}^{5} := \frac{1}{10}; \\
\gamma_{30}^{6} &:= \frac{6-2\mathsf{c}-3d_2}{30},\ \gamma_{31}^{6} := \frac{18+2\mathsf{c}+3d_2}{30},\ \gamma_{32}^{6} := \frac{1}{5}.
\end{aligned}$$